Conduction-based Charging Maps for Latent Heat Storages

B. Peremans[1,2], M. Blommaert[1,2,3], M. Baelmans[1,2]
[1]Department of Mechanical Engineering, KU Leuven, 3001 Leuven, Belgium
[2]EnergyVille, 3600 Genk, Belgium
[3]Flemish Institute for Technological Research (VITO), 2400 Mol, Belgium

Abstract

Charging of latent heat storages is hampered by the low PCM thermal conductivity. Moreover, the lack of design rules for LHSs complicates the development of commercial compact storages. In the present work, the combined charging power and storage density is presented for PCM storages enhanced by highly conductive aluminum fins, charged by a water flow with a finite total heat capacity, and dominated by conductive heat transfer in the PCM. The performance maps are valid for low temperature differences and small PCM enclosures, as for such designs effects of natural convection can be neglected. We show that the overall storage performance can be estimated from a unit cell approach which greatly reduces the computational effort. Moreover, reducing the individual compartment height as well as slowly and simultaneously charging the individual cells is demonstrated to be effective for increased charging performance.

Keywords: Latent heat storage, Phase change material, Performance maps, Metal fins.

1 Introduction

Latent heat storages are gaining more interest because of their capability of storing heat in a very compact way without the need of large temperature changes. During the melting or solidification of the Phase Change Material (PCM) a lot of heat is absorbed or released, with a limited temperature change, since the energy is stored as latent heat. However, these PCMs are typically characterized by a very low thermal conductivity, which greatly limits the charging capabilities of latent heat storages.

A lot of research has been performed on improving the heat transfer characteristics of latent heat storages by 1) incorporating highly conductive metal fin or foam structures and 2) methods as PCM encapsulation [1, 2]. The former approach creates highly conductive paths penetrating the PCM region, which easily conduct the heat between the source and PCM. In addition, the metal structures tend to divide the PCM region into smaller ones which results in lower heat diffusion lengths in the PCM. However, including metal structures into the storage reduces the overall storage capacity as part of the storage volume cannot be occupied by PCM.

Inserting highly conductive fins has been widely investigated both numerically and experimentally, with the most obvious fin structures being the plate fins and pin fins. Plate fins have been attached both to heated plates [3, 4, 5, 6, 7, 8] as heated tubes [9, 10] and have shown to be effective in increasing the charging performance of LHSs. Pin fins have been studied to a lower extent, and have been applied in a PCM-heat sink by Pakrouh et al. [11, 12]. Often, these studies are limited to parameter scans, comparing different fin lengths, widths, amount of fins, etc. Bejan et al. [13] studied T-shaped fin designs as a possible alternative for straight

fins. In the work of F. Jorissen [14], a tubular design with lots of small fins surrounding the tube was investigated (brush-like fin design). The high amount of small fins resulted in a good thermal contact between the PCM and heat source. However, the study was quite limited and lacks general conclusions on the concept's charging performance. More sophisticated fin designs were investigated by Pizzolato et al. in [15, 16] using a 2D and 3D topology optimization of a shell-and-tube LHS. The topology optimization led to completely new fin designs which are outperforming the traditional straight fins with respect to charging and/or storage performance. Despite that LHS design based on fins is a very promising concept, the numerous amount of studies are still lacking general design rules for fin lay-out, spacing, as well as overall storage design. Moreover, the dependency of the charging performance by simultaneously changing different design properties is often not explored or only to a low extent.

Metal foams are able to create small metal structures, and therefore very large heat transfer surfaces, and at the same time act as highly conductive fins for heat transfer enhancement. It has been reported that large reductions in charge time are achieved by using metal foams due to an increased overall thermal conductivity [17, 18, 19, 20]. For example, Bauer et al. [17] have shown an increase of the effective thermal conductivity from 0.17 W/mK to 5 W/mK for an aluminum foam with a porosity of 91%. Although compared to Li et al. [20], it is observed that the grain size of the foam greatly influences the charging performance of the storage. Despite the great gain in charging performance, due to the irregular shape of the foam, one might expect fin designs exist which may outperform these metal foams for the same storage capacity, e.g. based on the fin designs found by Pizzolato et al. [21].

PCM encapsulation simply encloses the PCM in capsules, often with a plastic shell [22, 23, 24]. The PCM capsules can have any kind of shape, but are frequently small spheres. The storage charging performance greatly benefits from reduced capsule size, as to reduce the thermal diffusion length inside the PCM. However, the storage capacity is reduced for spherical capsules by the inefficient stacking of the capsules and the particles shell volume.

Despite the abundance of individual studies, no general framework has so far been set-up for combined charging and storage performance of latent heat storages. Even more, overall design rules are still lacking, which hampers the translation into high performing commercial latent heat storages [25].

Therefore, this paper studies the general charging and storage trends for rectangular-shaped latent heat storages, enhanced by rectangular and uniformly spaced metal fins. By choosing rectangular shapes, the voids due to the inefficient stacking of individual spherical PCM capsules is omitted, therefore exploiting the full storage potential of the PCM. Further, uniformly spaced rectangular metal fins have well-known production techniques and are widely commercial available, which makes them attractive for economically feasible latent heat storage applications. Moreover, the charging maps are derived using a conduction-based model, which is valid for low temperature changes and small PCM enclosures, and which allows effects of natural convection to be neglected. However, due to the modular approach, the shape of the distributor and collector channels is still neglected in order to reduce the computational efforts in this first proof-of-principle demonstration.

The first section describes the internal structure of the studied latent heat storages, which consist of equally-sized PCM compartments separated by heat transfer fluid channels. Highly conductive fins are enhancing the heat transfer inside the PCM compartments. The second section studies the individual compartment charging and storage performance through dimensional analysis and by numerical simulations for different compartment shapes, heat supplies, amount of fins, and fin dimensions. The third section demonstrates the use of the performance maps of individual PCM compartments in the design and performance evaluation of a complete storage, and shows the importance of reduced compartment diffusion heights. The last section summarizes the main findings of this work.

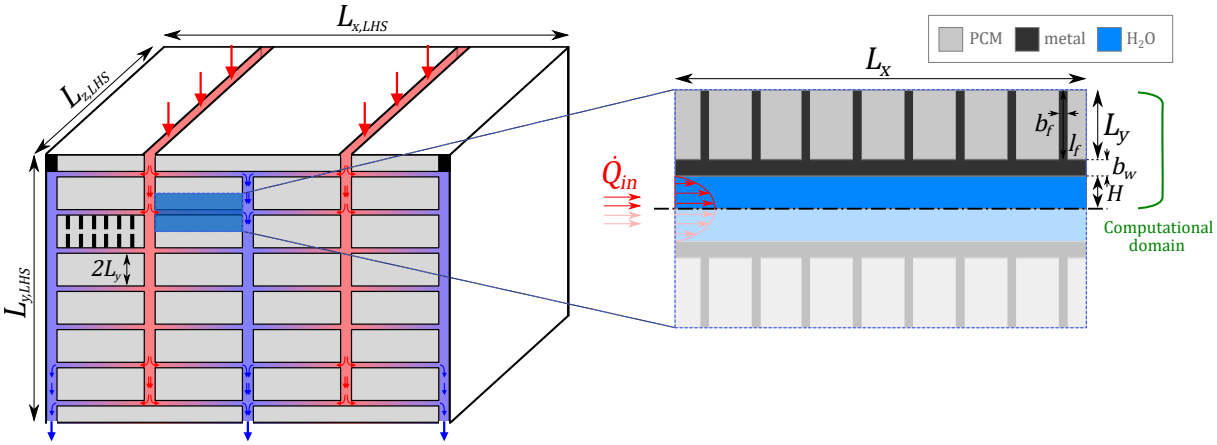

Figure 1: Overall storage (left) constructed as a stacking of individual rectangular compartments (right) with HTF channels in between.

2 The latent heat storage design

In this section, the structure of the latent heat storage is described. First, an overview of the complete storage is shown, which consists of different individual rectangular compartments. Secondly, an individual compartment is described in detail, comprising a heat transfer fluid (HTF) channel with on both sides PCM enhanced by metal fins.

2.1 Overall storage design

As was already pointed in previous section, we focus on achieving maximum storage capacity by considering storages with rectangularly shaped enclosures comprising the PCM. The rectangular shape ensures a compact stacking and guarantees control of the intermediate channel dimensions.

The latent heat storage considered is designed as a cuboid with lengths $L_{x,\mathrm{LHS}}$, $L_{y,\mathrm{LHS}}$, and $L_{z,\mathrm{LHS}}$ (see left side of Fig. 1). Rectangular distributor water channels are located at the top and collector channels have their outlets at the bottom of the storage. The distributor and collector channels are interconnected by smaller horizontal channels. In between, the voids are filled with PCM. The internal part of the storage is therefore constructed as a pile-up of individual rectangular cuboid PCM compartments. These individual PCM compartments either consist of pure PCM or a combination of PCM and highly conductive metal structures. The water flow surrounding the PCM compartments will deliver or extract heat depending on the moment of operation. A cross section of the storage is shown in Fig. 1.

The distributor and collector channels are assumed to be designed to generate a uniform distribution of the total flow rate over the different parallel horizontal channels. The design of these channels is, however, out of the scope of this work. Moreover, the modular design in Fig. 1 can be used to create different LHS designs by rearranging the individual compartments (e.g. to achieve a flat LHS instead of a cubic LHS) or to change the location and/or orientation of the flow distributor and collector.

2.2 Single compartment as computational domain

Since the vertical feed and collector channels are much wider than the horizontal channels, we can in a first instance neglect the temperature and pressure drops over these channels. This allows us to reduce the problem to the design of an individual storage unit as shown in the right part of Fig. 1. The individual unit is assumed to be an extrusion of a 2D design, and consists of

a single straight water channel, with on both sides a storage compartment. The water channel is a parallel plate channel with a rectangular cross section, with internal height $2H$. It is assumed that the water input heat $\dot{Q}_{in}$ with respect to the PCM melting temperature T_m is constant over time and water is always flowing from the left to the right. The power $\dot{Q}_{in}$ is mathematically defined as:

$$\dot{Q}_{in} = \dot{m} c_w \Delta T = \rho_w c_w \langle v \rangle H L_z (T_\infty - T_m). \tag{1}$$

The variables $\dot{m}$, $\langle v \rangle$, ρ_w, c_w and T_∞ are the mass flow rate, average flow velocity, density, specific heat capacity and input temperature of the water flow, respectively.

The PCM compartments have dimensions L_x and L_y and are enhanced by a limited amount of uniformly spaced rectangular metal fins, which are perpendicularly oriented to the heat supplying wall. It is assumed the metal fins are all equal in shape with width b_f and height l_f, and extend through the full PCM layer ($L_y = l_f$). The channel wall is characterized by a thickness b_w and is composed of the same material as used for the internal fin structure. The computational domain is modelled in two dimensions only, therefore neglecting any side effects in the third dimension. Due to the symmetry of the domain, only half of the water channel is modelled, and thus also only one PCM compartment (as indicated on the right side of Fig. 1). It allows to reduce the computational cost. A symmetry boundary condition is therefore imposed in the middle of the water channel.

The authors already described the performance of such single units extensively in [26] and [27]. This paper further elaborates the performance trends which were set up and provides the trends for real-sized metal fins. Several performance maps are constructed showing the combined storage and charging performance in function of the storage design. For given design constraints, the performance maps enable to select the most desirable configurations, i.e. satisfy the charging and storage demand. The design of the inlet flow distributor is out of the scope of this research. Nevertheless, several papers demonstrate that a uniform splitting of the flow across parallel channels is possible with appropriate distributor designs [28, 29]. Using the assumption that the incoming water is perfectly distributed over all units, the overall performance of the storage can be deduced by rescaling the unit performance using a dimensional analysis[1].

3 Performance maps for a single PCM compartment

In this section, the single PCM compartment is analysed by numerical simulations and its combined storage and charging performance is mapped for different configurations. First, the performance indicators that represent the storage capacity and charging power are defined. Secondly, the modelling equations are introduced, describing the heat transfer in the water channel, metal and PCM, as well as the phase change of the PCM. Thirdly, a dimensional analysis is set up, followed by a parameter reduction, and resulting in a general dependency amongst all dimensionless properties. Finally, the performance trends for PCM compartments enhanced by rectangular and uniformly distributed metal fins are set up for different compartment configurations. These performance trends are used in the next section to evaluate the performance of an overall LHS.

[1]Note that by individually applying the proposed procedure for all PCM compartments and by superimposing the storage and charging performance indicators (e.g. $e_L = \sum_i E_{L,i}/V_{tot}$, see next section, Eq. (2)), the performance of a storage charged by a non-uniformly distributed water flow across the parallel channels can also be estimated. However, the obtained charging performance will be a lower limit for the effective charging performance, as the enhancing influence of neighbouring PCM compartments due to uneven charging is not taken into account.

3.1 Performance characterization

Three main performance characteristics for latent heat storages are defined, based on the analysis the authors presented in references [26, 27]. The first measure is the storage density e which determines how much heat can be stored in a certain storage volume. We define two storage densities as:

$$e_L \triangleq \frac{E_L}{V_{tot}} = \rho \Delta h \frac{V_{\mathrm{PCM}}}{V_{tot}} \quad \text{and} \quad e_{LS} \triangleq \frac{E_{LS}}{V_{tot}} = \rho(\Delta h + c_{p,\mathrm{PCM}} \Delta T) \frac{V_{\mathrm{PCM}}}{V_{tot}}, \tag{2}$$

with V_{PCM} and V_{tot}, respectively, the PCM volume and the overall storage volume, and ΔT the temperature difference between the heat supply and the initial temperature of the storage. The latent storage density e_L only includes the total latent heat which can be stored. The overall storage density e_{LS} includes both sensible and latent heat. For small temperature differences ΔT, the share of sensible heat will be rather low with respect to the high latent heat of the PCM. Therefore, it is more convenient to look at the latent storage density only, which corresponds to completely melting or freezing the storage for heat and cold storage respectively.

Secondly, the charging performance of latent heat storages is characterized by its power density $\dot{q}$. Power density is the charging rate of a unit PCM volume. In other words. the higher the power density, the more heat or cold can be stored in a certain time span for a given storage volume. Mathematically, it is defined as the ratio of the mean power at which the PCM is charged over the total storage volume, according to

$$\dot{q} = \frac{\dot{Q}}{V_{tot}}, \tag{3}$$

with $\dot{Q}$ the mean PCM charging power. If the power density is only based on the power coming from the latent heat being stored, the power density is linked to the latent energy density by

$$\dot{q}_L = \frac{e_L}{t_{ch}}, \tag{4}$$

with t_{ch} the charge time, also the total time needed to melt or solidify all the PCM in the storage. A similar link cannot be found between power density and overall storage density as it would take an infinite amount of time for the storage to uniformly reach the temperature of the heat source. By numerically simulating the melting or solidification process, the time needed for completing the melting or solidification process, i.e. the charge time, is recorded. The direct link in Eq. (4) enables the power density, and thus the charging performance, to be calculated by only knowing the charge time of the storage.

Thirdly, as the charging power is limited to the input power of the heat source, we opt to transform the power density in a new charging performance indicator, i.e. the charging ratio σ, which takes into account this input power, as further shown. The charging ratio is defined as the ratio of stored heat to input heat:

$$\sigma = \frac{E}{E_{in}}, \tag{5}$$

with $E_{in} = \dot{Q}_{in} \cdot t_{ch}$ the accumulated energy input provided by the water flow at the storage inlet. The charging ratio determines the fraction of heat that could effectively be stored in the PCM and therefore always ranges between zero and one.

Assuming the water input power is constant over time, the charging ratio is rewritten in terms of power, i.e.:

$$\sigma = \frac{\dot{q} \cdot V_{tot}}{\dot{Q}_{in}}, \tag{6}$$

with the product $\dot{q} \cdot V_{tot}$ being the mean charging power of the storage compartment. Note that, just like in the definition of $\dot{q}$, the charging ratio can be defined based on the latent heat stored σ_L or the combined latent and sensible heat stored σ_{LS}, and that σ_L is easily deduced from the charge time using Eq. (4), i.e.:

$$\sigma_L = \frac{e_L}{t_{ch}} \cdot \frac{V_{tot}}{\dot{Q}_{in}}. \tag{7}$$

Before we focus on the three performance indicators storage density e, power density $\dot{q}$ and charging ratio σ, we describe the model used for estimating these parameters.

3.2 LHS Modelling

The storage compartment is described by two coupled models: 1) a heat transfer and phase change model for the PCM-metal region, and 2) a heat transfer and transport model for the heat-carrying water flow. A finite volume implementation of these model equations is used to solve the time-dependent heat transfer and phase change and for the estimation of the performance indicators described in Section 3.1.

PCM-metal It is assumed that the heat transfer in PCM is mainly conduction-driven because of the solid phase, and the inclusion of metal structures which are hampering natural convection to occur in the liquid phase. The heat transfer is therefore modelled by a transient heat conduction problem,

$$\rho \frac{\partial h}{\partial t} - \nabla \cdot k \nabla T = 0, \tag{8}$$

and solved using a finite volume technique, with h and T the enthalpy and temperature field, respectively, ρ the density and k the thermal conductivity. The transient term is put in the enthalpy formulation such that the melting and solidification of the PCM can be modelled by adding an enthalpy-temperature relation for PCM. The reference state for h is taken in the solid state at the melting temperature T_m. This equation couples the temperature to the enthalpy of the PCM through the following piecewise functional:

$$T = \begin{cases} T_m + \frac{h}{c_{p,\mathrm{PCM}}} & : h \leq 0 \\ T_m & : 0 < h < \Delta h \\ T_m + \frac{h - \Delta h}{c_{p,\mathrm{PCM}}} & : h \geq \Delta h \end{cases}, \tag{9}$$

with $c_{p,\mathrm{PCM}}$ the PCM specific heat capacity, and Δh the PCM latent heat of fusion, also known as the heat being absorbed or released during phase change. This formulation is the well-known enthalpy method for phase change modelling and is able to deal with a fixed melting temperature. The enthalpy method has the advantage of being easy to numerically implement and achieve high accuracy without the need of exactly tracking the phase change front. However, the computational cost rises due to the simultaneous solution of the heat conduction equation and the enthalpy equation, as well as its piecewise nature. For the metal the relationship is given by $h = c_p(T - T_m)$.

Heat transfer fluid The heat transfer in the water channel has a combined effect of conduction and advection. Therefore, the heat transfer in the water channel is modelled by a 1D height-averaged convection-diffusion equation, written as

$$\begin{aligned}\rho_w c_w \frac{\partial \langle T \rangle}{\partial t} + \langle \zeta \xi \rangle \frac{\partial}{\partial x}\Big[\rho_w c_w \langle v \rangle \langle T \rangle\Big] + (1 - \langle \zeta \xi \rangle) \frac{\partial}{\partial x}\Big[\rho_w c_w \langle v \rangle T_i\Big] \\ - \frac{\partial}{\partial x}\Big[k_w \frac{\partial \langle T \rangle}{\partial x}\Big] - k_w (\langle T \rangle - T_i)\Big\langle \frac{\partial^2 \xi}{\partial y^2} \Big\rangle = 0,\end{aligned} \tag{10}$$

which is obtained by averaging the full convection-diffusion equation in 2D over the height of the water channel [30]. $\zeta(y)$ and $\xi(y)$ are the imposed dimensionless velocity and temperature profile, respectively, and $\langle . \rangle$ the averaging operator. Therefore, $\langle T \rangle$ is the height-averaged water temperature and $\langle v \rangle$ the average flow velocity. The index w indicates the water properties, whereas i indicates the interface with the PCM domain. The flow is assumed to be fully hydrodynamically and thermally developed. Because the velocity profile is known for fully developed parallel plate flow, the height-averaging can effectively be used to reduce the computational cost. The imposed velocity and temperature profile result in a constant factor $\langle \zeta \xi \rangle = 1.224$ and a quadratic dependent factor $\left\langle \frac{\partial^2 \xi}{\partial y^2} \right\rangle = 2.307 H^2$.

Validity of the energy model By neglecting natural convection in the liquid PCM, the validity of the energy model and resulting performance maps are restricted to low temperature differences and small PCM enclosures. The Rayleigh number Ra [31] is defined as

$$Ra = \frac{g \beta (T_\infty - T_m) L^3}{\nu \alpha}, \tag{11}$$

with g the gravitational acceleration, β the coefficient of thermal expansion, T_∞ the supply temperature, T_m the PCM melting temperature, L the characteristic length of the PCM enclosure, ν the kinematic viscosity, and α the thermal diffusivity. The Rayleigh number gives an indication of the amount of natural convection that arises during the charging of the PCM. For $Ra > 10^3$, natural convection is clearly observed as reported in [32, 33]. However, for low Rayleigh numbers, natural convection is hampered, e.g. due to a low supply temperature difference $(T_\infty - T_m)$ or small PCM enclosure (L).

Further, the PCM is assumed to have a fixed melting point, and free of any supercooling and phase segregation. Moreover, we will employ the same properties for the PCM in both the solid and liquid phase, such that the energy model is applicable for both the charging and discharging cycle.

Lastly, the HTF energy model is restricted to developed incompressible and laminar flow in straight ducts. Any entrance effects are not taken into account. Moreover, height-averaging the convection-diffusion problem requires to impose a fixed dimensionless temperature profile across the streamwise direction, which is not an exact representation of the real physics. However, we expect the model to be representative for small water channels, as such that the water is in close contact with the PCM enclosures which will diminish the effect of the imposed profile.

3.3 Dimensional analysis

To obtain general case-independent design rules, a dimensionless framework is now set up by applying the Buckingham-Pi theorem. The dimensionless properties are constructed according to [26] for the compartment set up:

$$\bar{t}_{ch} = \frac{\alpha_{\text{PCM}} t_{ch}}{L_y^2}, \quad \bar{T} = \frac{T_m - T_0}{T_\infty - T_0}, \tag{12}$$

$$\text{AR}_{xy} = \frac{L_x}{L_y}, \quad \text{AR}_{zy} = \frac{L_z}{L_y}, \tag{13}$$

$$Ste = \frac{c_{p,\text{PCM}}(T_\infty - T_0)}{\Delta h_{\text{PCM}}}, \quad \text{and} \quad \Pi_L = \frac{L_y^2 \Delta h_{\text{PCM}}}{\alpha_{\text{PCM}}^2}, \tag{14}$$

with L_x, L_y, L_z the length in the x-, y- and z-direction, α_{PCM} the PCM thermal diffusivity[2], and T_0, T_m, T_∞ the initial temperature, the melting temperature of the PCM and the heat source supply temperature, respectively. $\bar{t}_{ch}$ is the dimensionless charge time, and is the equivalent of the dimensionless Fourier number. The temperature ratio $\bar{T}$ is a relative indication of the sensible heat needed upon phase change, with respect to the driving temperature force. Both aspect ratios AR_{xy} and AR_{zy} define the shape of the PCM compartment. For a 2D domain, the third dimension is interpreted as infinitely long and therefore $\text{AR}_{zy} \to \infty$. The Stefan number is the ratio of sensible heat to latent heat. The last dimensionless property Π_L relates the latent heat value to the PCMs diffusivity. The metal properties, i.e. metal density ρ_m, metal thermal conductivity k_m, and metal specific heat $c_{p,m}$, are included in the dimensionless framework by dividing the metal properties by the corresponding PCM properties, i.e.:

$$\bar{\rho}_m = \frac{\rho_m}{\rho_{\text{PCM}}}, \quad \bar{k}_m = \frac{k_m}{k_{\text{PCM}}}, \quad \text{and} \quad \bar{c}_{p,m} = \frac{c_{p,m}}{c_{p,\text{PCM}}}. \tag{15}$$

while the fin width b_f, the fin length l_f, number of fins N, and wall thickness b_w are transformed into dimensionless groups using:

$$\text{AR}_{fin} = \frac{b_f}{l_f}, \quad \bar{l}_f = \frac{l_f}{L_y}, \quad \phi = \frac{N \cdot b_f l_f}{L_x(L_y + H + b_w)}, \quad \text{and} \quad \phi_w = \frac{b_w}{L_y + H + b_w}, \tag{16}$$

with AR_{fin} the fin aspect ratio, ϕ the metal fin volume fraction, and ϕ_w the metal wall volume fraction. Note that, the dimensionless fin length is fixed, as it is assumed the fins extend through the full PCM layer, and therefore $\bar{l}_f = 1$ and $\text{AR}_{fin} = \frac{b_f}{L_y}$. Note that the dimensional analysis could easily be extended for $\bar{l}_f < 1$, however, this would require to take into account the additional dependency of the charging performance on $\bar{l}_f$. Also, the water flow properties are included: water density ρ_w, water thermal conductivity k_w, water specific heat c_w, average water velocity $\langle v \rangle$, and half channel height H. The water properties are easily transformed into non-dimensional groups by dividing its property by the corresponding PCM property, whereas the channel height is transformed in a water volume fraction, and the average water velocity is transformed into a Péclet number, i.e.:

$$\bar{\rho}_w = \frac{\rho_w}{\rho_{\text{PCM}}}, \quad \bar{k}_w = \frac{k_w}{k_{\text{PCM}}}, \quad \bar{c}_w = \frac{c_w}{c_{p,\text{PCM}}}, \quad \psi = \frac{H}{L_y + H + b_w}, \quad \text{and} \quad Pe = \frac{\langle v \rangle H}{\alpha_w}. \tag{17}$$

By initializing the storage on the melting temperature of the PCM, the dimensionless temperature becomes zero ($\bar{T} = 0$). Taking all these dimensionless properties into account, the general dependency amongst the 18 dimensionless properties is summarized as

[2]Recall that the thermal diffusivity is calculated as $\alpha = \frac{k}{\rho c}$.

$$\bar{t}_{ch} = f(\mathrm{AR}_{xy}, \mathrm{AR}_{zy}, \bar{T}, Ste, \Pi_L, \bar{\rho}_w, \bar{k}_w, \bar{c}_w, \psi, Pe, \bar{\rho}_m, \bar{k}_m, \bar{c}_{p,m}, \phi, \mathrm{AR}_{fin}, l_f, \phi_w),$$
$$\text{with} \quad \begin{cases} \mathrm{AR}_{zy} \to \infty \\ \bar{T} = 0 \\ \bar{l}_f = 1 \end{cases}. \tag{18}$$

This relation enables performance trends, by assessing $\bar{t}_{ch}$, to be generalized towards any specific operational context, and enables design trends to be rescaled to any storage size.

Next, the performance indicators are also transferred in dimensionless format. While $\bar{e}$ can be found from an algebraic expression

$$\bar{e} = \frac{e}{e_{max}} = \frac{V_{\mathrm{PCM}}}{V_{tot}} = 1 - (\phi + \phi_w + \psi). \tag{19}$$

$\bar{q}_L$ immediately follows from

$$\bar{\dot{q}}_L = \frac{\bar{e}}{\bar{t}_{ch}}. \tag{20}$$

Note that σ_L is already a non-dimensional property.

3.4 Parameter reduction

A parameter reduction is performed to further reduce the amount of dependencies that need to be accounted for to set up the charging trends (14 at this point), based on the findings in [27]. The dimensionless charge time was studied for a rectangular PCM compartment charged by a water flow with a constant input power, which showed a remarkable linear trend with the compartment aspect ratio AR_{xy}. More specifically, the slope was shown to scale inversely proportional with respect to the Péclet number Pe. Therefore a new dimensionless parameter is proposed which captures both effects of the aspect ratio and Péclet number. The new dimensionless property τ is based on the ratio of maximum storage capacity to input heat, i.e. $E/\dot{Q}$-ratio and is mathematically expressed as

$$\tau \triangleq \frac{\alpha_{\mathrm{PCM}}}{L_y^2} \cdot \frac{E}{\dot{Q}_{in}}. \tag{21}$$

Note that the $E/\dot{Q}$-ratio has dimensions of time. Therefore, the corresponding dimensionless time scale τ is constructed in the same way as the dimensionless charge time $\bar{t}_{ch}$ (see Eq. (12)). By rewriting Eq. (21) using Eq. (1) and (2) as follows

$$\tau \triangleq \frac{\alpha_{\mathrm{PCM}}}{L_y^2} \cdot \frac{E}{\dot{Q}_{in}}, E = \rho_{\mathrm{PCM}}(\Delta h + c_{p,\mathrm{PCM}}(T_\infty - T_0))V_{\mathrm{PCM}}, \dot{Q}_{in} = \rho_w c_w \langle v \rangle H L_z (T_\infty - T_0)$$
$$\Rightarrow \tau = \frac{k}{\rho c_p}\bigg|_{\mathrm{PCM}} \cdot \frac{1}{L_y^2} \cdot \frac{\rho_{\mathrm{PCM}}\big(\Delta h + c_{p,\mathrm{PCM}}(T_\infty - T_0)\big) L_x L_y L_z}{\rho_w c_w \langle v \rangle H L_z (T_\infty - T_0)}$$
$$= \frac{k_{\mathrm{PCM}}}{k_w} \cdot \frac{L_x}{L_y} \cdot \frac{k_w}{\rho_w c_w \langle v \rangle H} \cdot \frac{1 + \frac{c_{p,\mathrm{PCM}}(T_\infty - T_0)}{\Delta h}}{\frac{c_{p,\mathrm{PCM}}(T_\infty - T_0)}{\Delta h}},$$

τ is shown to be not an independent parameter and is derived from the other dimensionless properties as

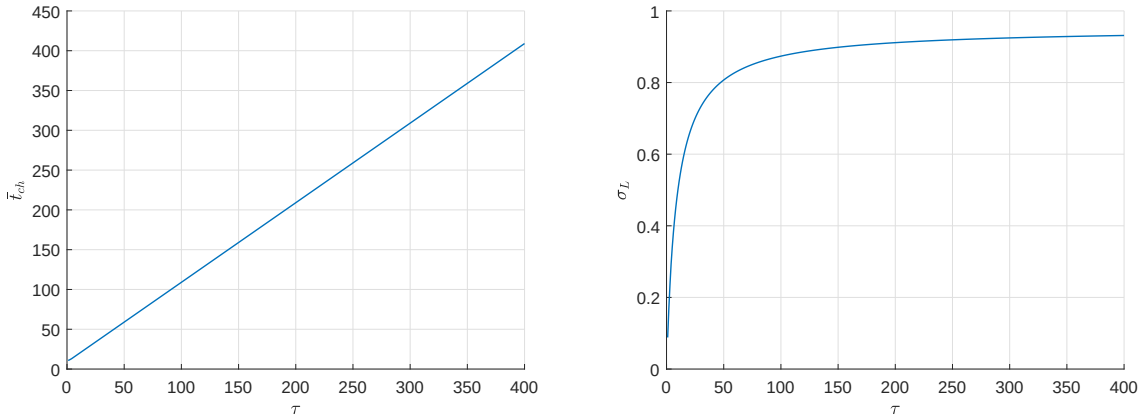

(a) Dimensionless charge time in function of the dimensionless time scale τ for $Ste = 0.05$.

(b) Latent charging ratio in function of the dimensionless time scale τ for $Ste = 0.05$.

Figure 2: Dimensionless charge time $\bar{t}_{ch}$ and charging efficiency σ as a function of the dimensionless time scale τ.

$$\tau = \frac{\mathrm{AR}_{xy}}{Pe} \cdot \frac{1 + Ste}{\bar{k}_w Ste}. \tag{22}$$

The evolution of the dimensionless charge time and charging ratio is shown with respect to τ in Fig. 2(a) and 2(b), respectively, for a PCM domain without fins and a Stefan number of $Ste = 0.05$. The performance lines for different Péclet numbers show a remarkable similarity as they almost coincide, and therefore only one curve is shown. As a result, the time scale τ reduces the amount of dependent dimensionless properties, since both the domain aspect ratio and Péclet number dependencies are captured simultaneously. Recall the definition of the charging ratio Eq. (7), which is rewritten in terms of dimensionless properties as

$$\sigma_L = \frac{1}{1 + Ste} \cdot \frac{\tau}{\bar{t}_{ch}}. \tag{23}$$

As the latent charging ratio follows from the dimensionless charge time, the charging ratio trend is also generalized (see Fig. 2(b)). In other words, the dependency of the charging ratio on the water Péclet number and PCM domain aspect ratio is reduced to one single dependency. This brings the number of parameters to determine the performance indicators to 13: τ, Ste, Π_L, 6 relative material properties for fluid and metal, ψ, ϕ_m, AR_{fin} and ϕ_w.

Note that, although not visible in the performance trends, (1) the dimensionless charge time trend flattens for small aspect ratios (in the region $\mathrm{AR}_{xy} < 2$), and (2) both performance lines, i.e. the dimensionless charge time and charging ratio as a function of τ, for different Péclet numbers do not match exactly[3]. This means that although a single parameter reduction could be carried out, this comes at the expense of an additional, though small, model error. It was found that the trends have a slight vertical offset with respect to each other, with a maximum absolute deviation on σ_L of 3.38% in the range of $1.81 < Pe < 28.97$.

[3]The performance trends $\tau - \bar{t}_{ch}$ have a slight lower vertical offset for lower Péclet numbers, resulting in a small increase in performance. This was exploited in [27] by simultaneously reducing the compartment aspect ratio and water Péclet number, by means of parallelly chargeable compartments.

3.5 Dimensionless performance maps

We have studied the performance trends with respect to energy density and power density for PCM enhanced by infinitely thin metal fins already in [26] by means of PCM-metal composites. These trends were designated as the charging limits, as they show the highest performance of latent heat storages enhanced by uniformly spaced rectangular fins. As infinitely thin fins are not manufacturable in practice, we introduce the consequences of having finite-sized fins on the performance maps in this section. To limit the computational effort, the calculations in this paper are all performed under conditions of Eq. (18), with metal properties $\bar{\rho}_m = 2.7$, $\bar{k}_m = 1025$, $\bar{c}_{p,m} = 0.88$, and fluid properties $\bar{\rho}_w = 1$, $\bar{k}_w = 2.9$, $\bar{c}_w = 4.2$, with a fixed Stefan number $Ste = 0.05$, an infinitely small water channel[4] $\psi \to 0$, and a fixed channel wall thickness $\phi_w = 0.0005$.

The Stefan number has been fixed as the charging performance trends as a function of the Stefan number are well reported in literature (see [26, 27]). These conclusions still hold and are summarized as: 1) increasing the temperature difference between the water supply and PCM melting temperature increases the charging performance due to higher temperature gradients, and thus faster conduction, and 2) the power density increases for increased ratio of PCM melting heat to PCM heat capacity (i.e. $\frac{\Delta h}{c_{p,\mathrm{PCM}}}$), as this allows steeper temperature gradients at the PCM melting front to be generated. In this example, the Stefan number has been chosen to represent a PCM (paraffin) charged by a low temperature difference ($\Delta T \approx 10°C$).

Following from the dimensional analysis in Eq. (18), the remaining properties of interest which influence the LHS storage and charging performance are the PCM domain aspect ratio AR_{xy}, the water Péclet number Pe, the metal volume fraction ϕ and the metal fin aspect ratio AR_{fin}. Recall also that the influence of $\mathrm{AR}_{\mathrm{PCM}}$ and Pe is combined in the dimensionless time scale τ (see Eq. (22)). Therefore, we aim at setting up performance maps for different values of τ, ϕ and AR_{fin}. In principle, the performance maps can be easily extended further using the dimensionless framework in Section 3.3 by varying more of the simulation parameters, e.g. choosing a different PCM (affecting Ste, Eq. (15), (17)) or a different metal (affecting Eq. (15)), choosing a different supply temperature (affecting Ste), etc. Moreover, the authors verified that the design guidelines resulting from the dimensionless performance trends for different sets of dimensionless properties are similar to the ones presented in this section, given that $\bar{k}_m \gg 1$, i.e. the metal has a much higher thermal conductivity than the PCM, which is usually a valid assumption. In other words, similar charging performance vs. storage performance profiles (as will be shown in Fig. 3 and Fig. 4) are found. However, it should be stressed that the numerical values of the dimensionless charging performance and charging ratio will be different. As a result, the performance trends in this work are used to set up general design guidelines for high performing LHSs with highly conductive fins, rather than presenting a multitude of application specific performance trends which could be of use for a quick lookup of the LHS performance.

Performance maps First, the charging trends are set up in terms of storage density and power density. Fig. 3 shows the combined storage and charging performance in dimensionless format ($\bar{e}$ and $\bar{q}_L$) for different dimensionless time scales τ and different fin aspect ratios AR_{fin}. The performance indicators are shown in a way configurations closer to the origin of the axis have a higher performance. Recall that $\tau \sim \frac{\mathrm{AR}_{xy}}{Pe}$ captures both the module shape as well as the input power of the water flow. Each performance chart is valid for a fixed τ with different performance lines corresponding to different fin aspect ratios. As a result, all performance trends consist of a Pareto front (solid lines), and a Pareto-dominated part (dashed lines). The latter corresponds to configurations that are less optimal than at least one configuration on the Pareto front. In this case, we see that for these dominated configurations, a configuration on the Pareto front can be found with the same charging performance, but with an elevated storage capacity.

[4]For more information on this assumption, the reader is referred to [27]

It should be noted that the zero point $1 - \bar{e} = 0$ is always part of the Pareto front. This point corresponds to a compartment solely filled with PCM. Thus, the same point is always reached on the vertical axis, independent of the fin geometry.

The solid lines clearly indicate that introducing metal fins is beneficial for the charging performance, i.e. the power density $\bar{\dot{q}}_L$ and charging ratio σ_L both increase for higher metal fin fractions. However, notice that the storage capacity reduces due to the lower PCM volume fraction $\bar{e}$. Therefore, there exists a turning point at which the power density starts decreasing (i.e. the dashed lines). Notwithstanding that these storage configurations are charged faster (lower charge time t_{ch}), their power density drops as the additional heat transfer enhancement does not outweigh the reduction in storage capacity. Moreover, for configurations with high aspect ratio fins ($AR_{fin} > 0.1$), a rather small region (left dashed line, where $1 - \bar{e} \in (0, \delta]$, with δ small) exists where the charging performance decreases, due to the very low amount of fins.

The Pareto fronts in Fig. 3 show an increase in charging performance, expressed by the dimensionless power density $\bar{\dot{q}}$, for an elevated presence of metal fin structures, although an associated decrease in storage capacity is found. The trends also indicate that lower fin aspect ratios are beneficial for the charging performance, since an increased number of small fins allows a better heat distribution than a limited number of big fins. For a fixed τ, the highest charging performance is reached for $\mathrm{AR}_{fin} \to 0$, which means the fin thickness approaches zero and the amount of fins goes to infinity. This is fully in accordance with the findings in [26]. As such, the performance characteristics for a PCM-metal composite described in that paper still function as an upper performance limit. For decreasing values of τ, the charging performance increases. This means that, on the one hand, the higher the input power of the water flow, the faster the PCM is being charged. On the other hand, the lower the compartment aspect ratio in terms of lowering the compartment length, the higher the power density becomes as the power per unit volume increases.

The charging performance is now studied by the latent charging ratio σ_L to investigate the effectiveness of storing the available heat (see Eq. (23)). Fig. 4 shows the transformed combined storage and charging performance in dimensionless format ($\bar{e}$ and σ_L) for different dimensionless time scales τ and different fin aspect ratios AR_{fin}. For a fixed τ, the charging ratio clearly increases for low fin aspect ratios, due to the elevated charging power. However, decreasing τ reduces the charging ratio. Indeed, although the charging power and thus the speed of charging increases due to the elevated water input power, a lower fraction of the applied heat can effectively be stored. In other words, efficiently storing the available heat is only possible if the storage is designed such that the storage compartment can be charged sufficiently slow.

Performance limits Fig. 3 already showed the increased power density for reduced τ. In the limit of $\tau \to 0$, the highest charging power is reached for any fin configuration. However, as $\tau \sim \frac{\mathrm{AR}_{xy}}{Pe}$ this implies either: 1) an infinite compartment input power $\dot{Q}_{in}$, 2) an infinitely small compartment length L_x, and/or 3) an infinite compartment height L_y. Both the first and second case ensure that the interface between the channel and PCM is at a constant temperature, which is the supply temperature T_∞. However, as the input power goes to infinity and/or the PCM volume approaches zero, the charging ratio drops to zero. The third case results in an infinite charge time due to the infinite amount of PCM and increased diffusion height, again resulting in a charging ratio dropping to zero. Therefore, the σ_L-trend for $\tau \to 0$ is not shown in Fig. 4, as it is rather trivial. Although they show the highest dimensionless charging power for all fin configurations, these set-ups are also the least effective in storing the available heat.

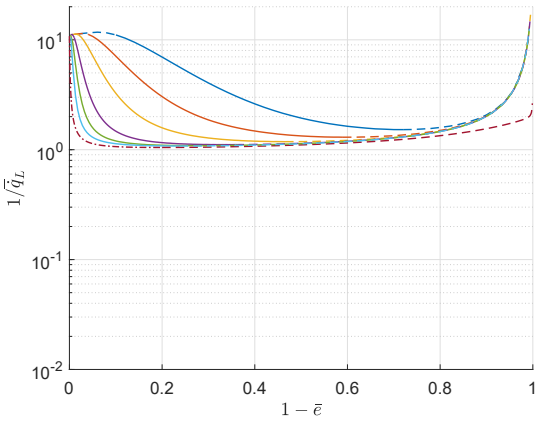

(a) $\tau = 1$.

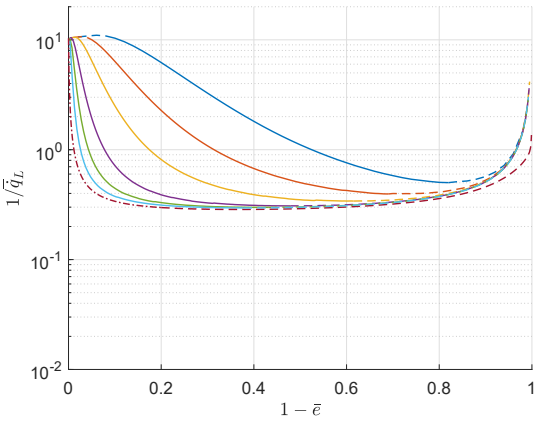

(b) $\tau = 1/4$.

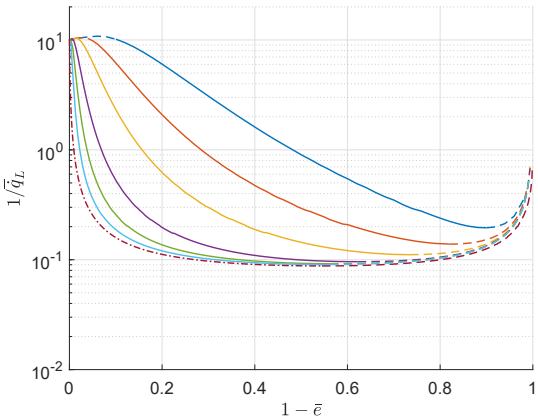

(c) $\tau = 1/16$.

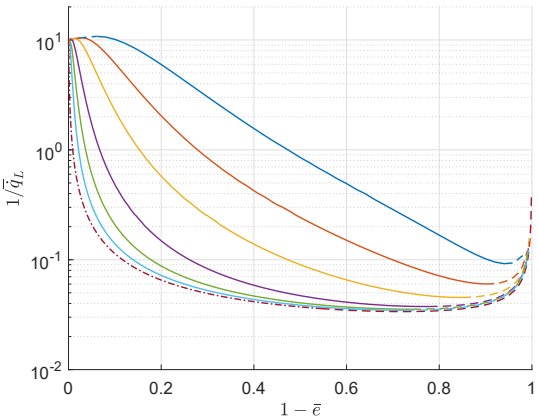

(d) $\tau = 1/64$.

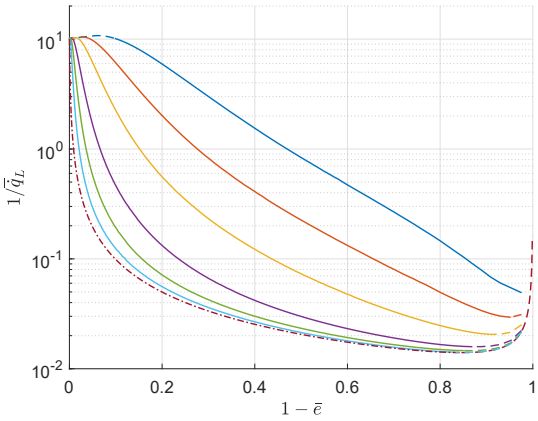

(e) $\tau \to 0$.

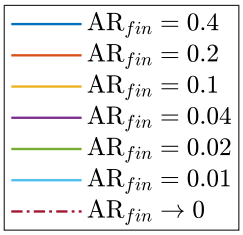

(f) Legend.

Figure 3: Performance trends for latent heat storages enhanced by finite-sized rectangular aluminum fins with aspect ratio AR_{fin} for fixed dimensionless time scale τ. The solid line shows the Pareto optimal solutions, while the dashed lines are Pareto-dominated configurations (another configuration can be found on the solid line with equal charging performance but higher storage capacity).

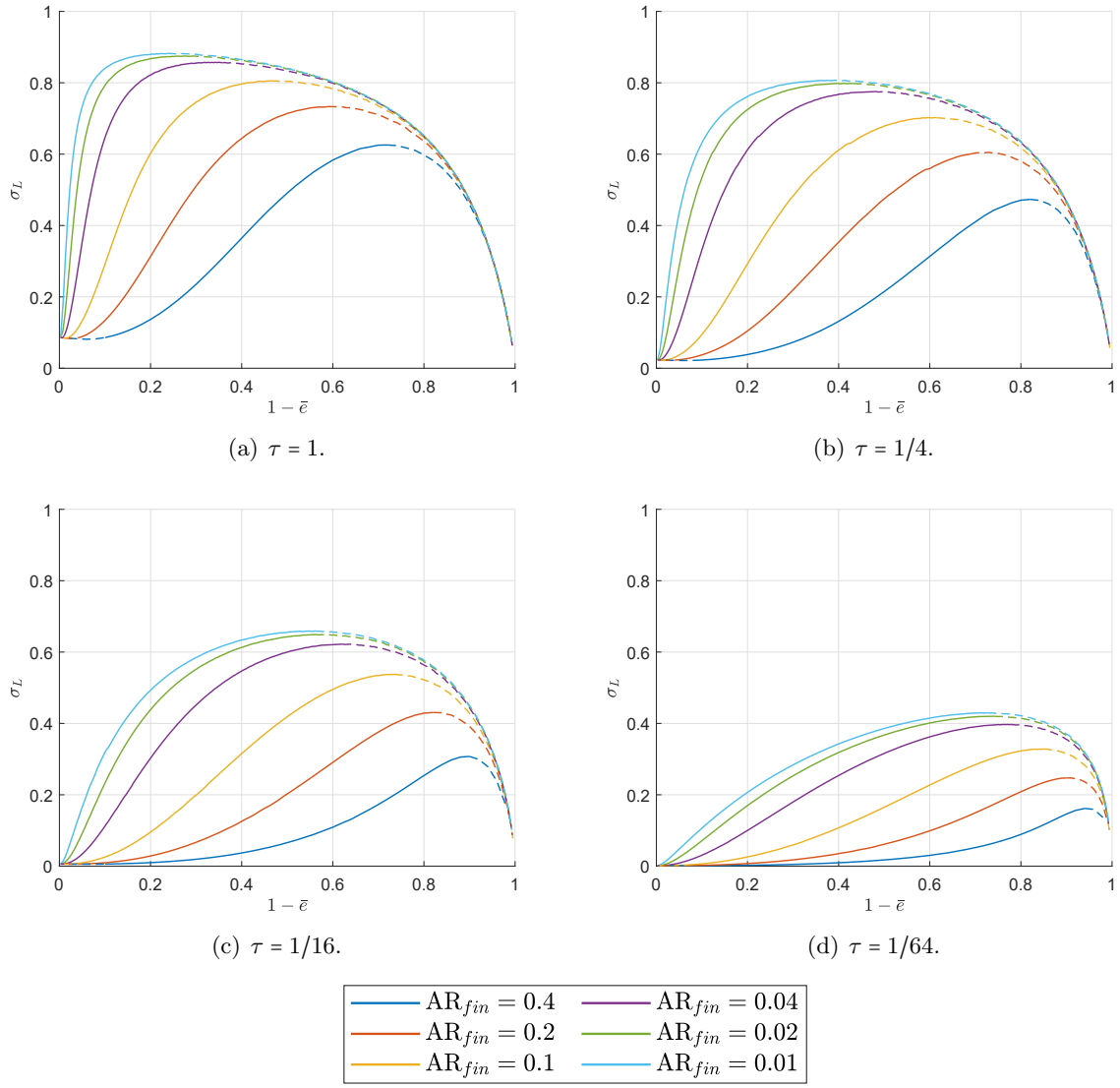

(a) $\tau = 1$.

(b) $\tau = 1/4$.

(c) $\tau = 1/16$.

(d) $\tau = 1/64$.

(e) Legend.

Figure 4: Charging ratio trends for latent heat storages enhanced by finite-sized rectangular aluminum fins with aspect ratio AR_{fin} for fixed dimensionless time scale τ. The solid line shows the Pareto optimal solutions, while the dashed lines are Pareto-dominated configurations (another configuration can be found on the solid line with equal charging performance but higher storage capacity).

4 Design and performance calculation of the LHS

The performance of LHS compartments enhanced by highly conductive and uniformly spaced metal fins was extensively studied in the previous section. This section will use the performance maps of a single compartment to design a complete LHS for maximum performance, which is constructed with equally sized individual compartments. In addition, we derive its overall charging and storage performance. First, the performance calculation of the overall storage is introduced. Afterwards, we analyse what the best configuration is of the unit compartments in the storage device. Next, the individual compartments are designed for maximum performance. Finally, the proposed design rules are applied to an example case that demonstrates the applicability and performance gain.

4.1 Overall storage performance

The internal structure of the overall storage was already introduced in Section 2, where the LHS was shown as a pile-up of individual PCM-metal compartments (see Fig. 1). The performance of the complete storage is now deduced, based on the approximations introduced in Section 2.2, by using the performance maps of the individual compartments.

As the heat transfer over the vertical side walls of individual cells is neglected, the power of a single compartment is calculated by using the performance maps in dimensionless format $\bar{\dot{q}}_L$ as

$$\dot{Q}_{sc} = \dot{q}_L V_{sc} = \frac{\bar{\dot{q}}_L \alpha_{\mathrm{PCM}} \rho_{\mathrm{PCM}} \Delta h_{\mathrm{PCM}}}{L_y^2} \Big(2L_x (L_y + H + b_w) L_z \Big), \tag{24}$$

with the subscript sc indicating the single compartment, and with $\bar{\dot{q}}_L$ defined by Eq. (4). Recall the storage structure in Fig 1, which shows the storage as a stacking of equally shaped compartments in the x- and y-direction. The number of compartments n of the storage is calculated as the product of the amount of compartments in the x- and y-direction, and is therefore related to the dimensions of the storage and compartment according to

$$n = \frac{L_{x,\mathrm{LHS}}}{L_x} \frac{L_{y,\mathrm{LHS}}}{2(L_y + H + b_w)}. \tag{25}$$

By perfectly distributing the available heat over the different compartments, the half-compartment input power is:

$$\dot{Q}_{in} = \frac{\dot{Q}_{in,tot}}{2n}, \tag{26}$$

which is the power imposed in the numerical simulations (see Section 2.2), and with $\dot{Q}_{in,tot}$ the total input power of the storage. The mean charging power of the overall storage until complete melting follows from the average compartment power and number of compartments as follows:

$$\dot{Q} = n\dot{Q}_{sc} = (\alpha_{\mathrm{PCM}} \rho_{\mathrm{PCM}} \Delta h_{\mathrm{PCM}}) \frac{V_{\mathrm{LHS}}}{L_y^2} \bar{\dot{q}}. \tag{27}$$

Eq. (27) clearly shows the dependency of the charging power on the dimensionless compartment charging density, which is determined by the design of the individual compartment. Again, the $\frac{1}{L_y^2}$-dependency arises which will crucially influence in the choice of design. To easily compare the performance of different designs, the charging ratio is again employed, which follows from the overall power as

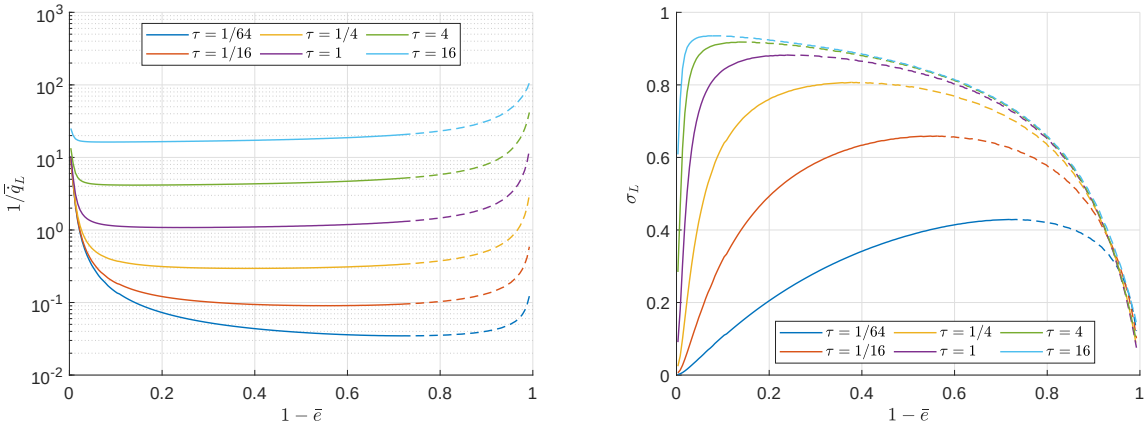

(a) Dimensionless power density $\bar{\dot{q}}_L$.

(b) Charging ratio σ_L.

Figure 5: Performance trends for a fixed fin aspect ratio of $\mathrm{AR}_{fin} = 0.01$ and for varying dimensionless time scale τ.

$$\sigma = \frac{\dot{Q}}{\dot{Q}_{in,tot}} = \frac{2n \cdot \dot{Q}_{sc}}{2n \cdot \dot{Q}_{in}} = \sigma_{sc}. \tag{28}$$

Note that the charging ratio equals the individual compartment charging ratio, as long as the total heat is equally divided over all compartments, and all compartment are equally designed. The former highlights the role of the distributor and collector design. The latter indicates that further flexibility can be introduced for inhomogeneous settings, when the design is limited in creating a uniform input heat over the individual compartments. For the cubic configuration studied here, the homogeneous input heat is assumed. As a result, in order to maximize the charging power of the overall storage, the individual compartments should be designed for maximum charging ratio.

4.2 What is the best configuration?

As the LHS is split up into n compartments, one can adjust the sequence in which the individual compartments are charged. It will, however, be shown that simultaneously charging the compartments and thus equally dividing the available input power over all compartments is the best way of charging the storage[5]. To more easily demonstrate this, the performance trends of Fig. 3 and 4 for a fin aspect ratio $\mathrm{AR}_{fin} = 0.01$ have been regrouped in Fig. 5.

Charging the compartments one-by-one results in a lowered global charging ratio, as the full input power is used to charge each compartment. The high power leads to a high water Péclet number, and thus a reduced dimensionless time scale τ (see Eq. (22)), which results in a decrease in charging ratio, as demonstrated in Fig. 2(b) and 5(b). However, the individual compartments temporarily reach a high charging power, as can be seen in Fig. 2(a) (recall that $\bar{\dot{q}} = \frac{\bar{e}}{\bar{t}_{ch}}$) and Fig. 5(a) for low values of τ, but nevertheless are not able to efficiently store the available heat. Splitting up the total input power equally over all compartments, reduces the water Péclet number by a factor n (recall that $Pe = \frac{\langle v \rangle H}{\alpha_w}$, and $\dot{Q}_{in} = \frac{\dot{Q}_{in,tot}}{2n} \sim \langle v \rangle H$). As a result, according to Eq. (22), the dimensionless time scale τ increases by a factor n (i.e. the amount of compartments), leading to a decrease of the individual compartment mean charging power:

[5]The available input power is equally divided over the parallel channels by equally splitting the input flow rate over the different channels. A suitable inlet distributor design might be required which is, however, out of the scope of this paper, but can be inspired by the work in [28, 29].

$$\forall n \in \mathbb{N}, n > 1 : \dot{Q}_{\parallel} = \dot{Q}_{sc}(\mathrm{AR}_{fin}, n\tau) < \dot{Q}_{sc}(\mathrm{AR}_{fin}, \tau) = \dot{Q}_{1\mathrm{by}1}, \tag{29}$$

with $\dot{Q}_{\parallel}$ and $\dot{Q}_{1\mathrm{by}1}$ the mean charging power of an individual compartment during parallel charging and serial charging, respectively. However, the mean power of the storage is the accumulated mean power of the individual parallel charged compartments, according to Eq. (27), and is found to be higher then the mean charging power of the serial charged storage:

$$n\dot{Q}_{\parallel} > \dot{Q}_{1\mathrm{by}1}. \tag{30}$$

This follows from the increased charging ratio for increased dimensionless time scale τ as demonstrated in Fig. 2(b) and 5(b), i.e.:

$$\forall \bar{e} : \sigma(\mathrm{AR}_{fin}, n\tau) > \sigma(\mathrm{AR}_{fin}, \tau) \quad \text{, with} \quad n > 1. \tag{31}$$

and therefore

$$\sigma_{\parallel} = \frac{n\dot{Q}_{\parallel}}{\dot{Q}_{in}} > \frac{\dot{Q}_{1\mathrm{by}1}}{\dot{Q}_{in}} = \sigma_{1\mathrm{by}1}. \tag{32}$$

In other words, charging the compartments in parallel results in a slow individual charging of the compartments, but an increased overall charging performance due to the accumulation of individual charging powers.

4.3 Designing the compartments for maximum charging ratio

The LHS is designed as a stacking of equally charging compartments. The design of the individual compartments is now optimized for maximum charging ratio, and determines the overall structure of the LHS.

Compartment height reduction The most important parameter to increase the charging performance of the storage is the compartment height L_y. Reducing the compartment height simultaneously increases the amount of compartments (see Eq. (25)) and reduces the individual compartment input power (see Eq. (26)), resulting in a quadratic increase in the dimensionless time scale τ. Increasing the dimensionless time scale while keeping the fin aspect ratio fixed, effectively increases the charging ratio, as was demonstrated in Eq. (31) and Fig. 2(b) and 5(b). This clearly demonstrates the advantage of using dimensionless properties as both parallel charging (see previous section) and the reduction of the compartment height are captured by one property, i.e. the dimensionless time scale τ. Mathematically formulated, decreasing the compartment height by a factor β results in:

$$\forall \bar{e} : \sigma(\mathrm{AR}_{fin}, \tau) < \sigma(\mathrm{AR}_{fin}, \beta^2\tau) \quad \text{, with} \quad \beta > 1. \tag{33}$$

Note that by keeping AR_{fin} fixed, we analyze a situation where the fins tend to shorten and narrow for reduced compartment height to keep the same fin aspect ratio by scaling the fin width b_f proportionally to L_y. It is clear that the lower the fin aspect ratio, the higher the charging ratio (see Fig. 4):

$$\forall \bar{e} : \sigma(\mathrm{AR}_{fin}, \tau) < \sigma(\gamma\mathrm{AR}_{fin}, \tau) \quad \text{, with} \quad 0 \leq \gamma < 1. \tag{34}$$

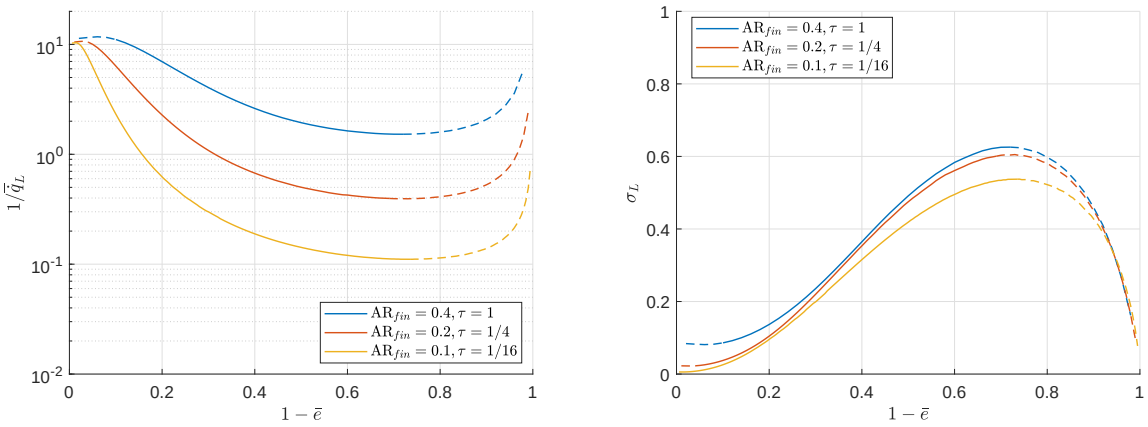

(a) Dimensionless power density $\bar{q}_L$.

(b) Charging ratio σ_L.

Figure 6: Performance trends for varying compartment height and fixed fin width.

However, by lowering the compartment height for a fixed fin aspect ratio, one might hit the minimum feasible fin width. Assume the fin dimensions are restricted by a minimum width $b_{f,min}$. Then Eq. (33) is used until $b_f = b_{f,min}$. Further reducing the compartment height would imply increasing the fin aspect ratio, as b_f is fixed to its minimum (recall $\mathrm{AR}_{fin} = \frac{b_f}{L_y}$). Taking into account the quadratic change of the dimensionless time scale τ with respect to the compartment height (see Eq. (33)), the performance change shows, despite of the fin aspect ratio increase, an increase in the charging ratio, and therefore:

$$\forall \bar{e} : \sigma(\mathrm{AR}_{fin}, \tau) < \sigma(\beta \mathrm{AR}_{fin}, \beta^2 \tau) \quad \text{, with} \quad \beta > 1. \tag{35}$$

This is also demonstrated in Fig. 6, which shows a selection of performance trends of Fig. 3 and 4 with a linear increase in fin aspect ratio and quadratic increase in dimensionless time scale. In other words, it is demonstrated that shortening the fins together with reducing the compartment height is an effective way of increasing the storage charging performance. Note that the charging performance increase of Eq. (35) is less pronounced then for fixed fin aspect ratios, i.e. Eq. (33).

Compartment length reduction Reducing the compartment length simultaneously increases the number of compartments, as indicated in Eq. (25) and also reduces the individual compartment input power (see Eq. (26)). As the compartment length and compartment input power scale proportionally, the dimensionless time scale τ is unaffected. As a result, the charging performance remains unchanged by varying the compartment length. Nevertheless, increasing the number of compartments by reducing the compartment length is beneficial for the overall channel pressure drop.

It should be noted, however, that the influence of the vertical distributor and collector channels becomes more pronounced for lowered compartment lengths. As the influence of these channels is neglected, care should be taken by interpreting the results for low aspect ratio compartments.

4.4 Example case

To demonstrate the applicability of the performance maps, a design example is given. The example consists of a square LHS with dimensions $L_{x,\mathrm{LHS}} = L_{y,\mathrm{LHS}} = L_{z,\mathrm{LHS}} = 0.5$ m. Assume the compartment size and metal fin width have lower manufacturing limits $L_{y,min} = 0.01$ m and

$b_{f,min}$ = 0.0001 m, and the heat source is at a supply temperature difference $\Delta T = T_\infty - T_m$ = 10°C. Using the performance trends of single compartments presented in this paper, the LHS can be designed for maximum charging and storage performance.

One compartment First, suppose the storage consists of a single compartment charged by an input power[6] $\dot{Q}_{in,tot}$ = 336 W only, i.e. a single HTF channel with on both sides a storage compartment (n = 2). Then, using Eq. (1), (13), (17), and (22), the PCM compartment is characterized by

$$\dot{Q}_{in} = \left.\frac{\dot{Q}_{in,tot}}{2n}\right|_{n=1} = 168 \text{ W}, \tag{36}$$

$$\text{AR}_{xy} = \frac{0.5 L_{x,\text{LHS}}}{L_{y,\text{LHS}}} = 2, \tag{37}$$

because the HTF channel is in the middle of the cubical storage,

$$Pe = \frac{\langle v \rangle H}{\alpha_w} = \frac{\dot{Q}_{in}/_{\rho_w c_w L_z (T_\infty - T_m)}}{\alpha_w} = 57.93, \tag{38}$$

and

$$\tau = \frac{\text{AR}_{xy}}{Pe} \cdot \frac{1 + Ste}{\bar{k}_w Ste} = \frac{1}{4}. \tag{39}$$

Knowing the dimensionless time scale τ, the charging performance is easily deduced from the charging maps in Fig. 3 and 4. For the convenience of the reader, the required performance trends are redrawn in Fig. 7. Without inserting metal fins, the charging ratio of the storage becomes very small ($\sigma_L \approx 2.28\%$, see Fig. 7(a) for n = 1 and Fig. 7(b) for $\bar{e}$ = 1), due to the high heat diffusion length in the PCM. Inserting low aspect ratio fins (AR_{fin} = 0.01), increases the charging ratio at the cost of a lowered storage capacity, up to a charging ratio of $\sigma_L = \pm 0.807$ for a storage capacity reduction of almost 40% ($\bar{e} \approx 0.61$, see Fig. 7(b)). Lowering the storage input power increases the parameter τ, which would shift the storage towards compartments with higher charging performance (see Fig. 7(a) and 7(b)). This clearly shows the need for reducing the compartment diffusion length, creating parallelly charging compartments, and thus slowly charging individual compartments.

N compartments Therefore, we consider now a storage consisting of n equally shaped compartments charged by the same total input power of $\dot{Q}_{in,tot}$ = 336 W. As the charging trends indicated that the individual compartment height should be as small as possible for increased charging performance, the compartment height is set to its minimum value: $L_y = L_{y,min}$. Recall that the compartment lengths are not influencing the charging performance significantly. Therefore, they are simply set to the overall storage length: $L_x = L_{x,\text{LHS}}$. The number of compartments and compartment input power follow from Eq. (25) and (26): n = 25, $\dot{Q}_{in}$ = 6.72 W. In dimensionless format using Eqs. (13), (17), and (22), the compartments are characterized by

$$\text{AR}_{xy} = \frac{L_{x,\text{LHS}}}{L_{y,min}} = 50, \tag{40}$$

[6]Note that the input power is chosen such that the combined charging and storage performance is easily derived from the limited set of performance maps, i.e. Fig. 3 and Fig. 4, without the need for interpolation.

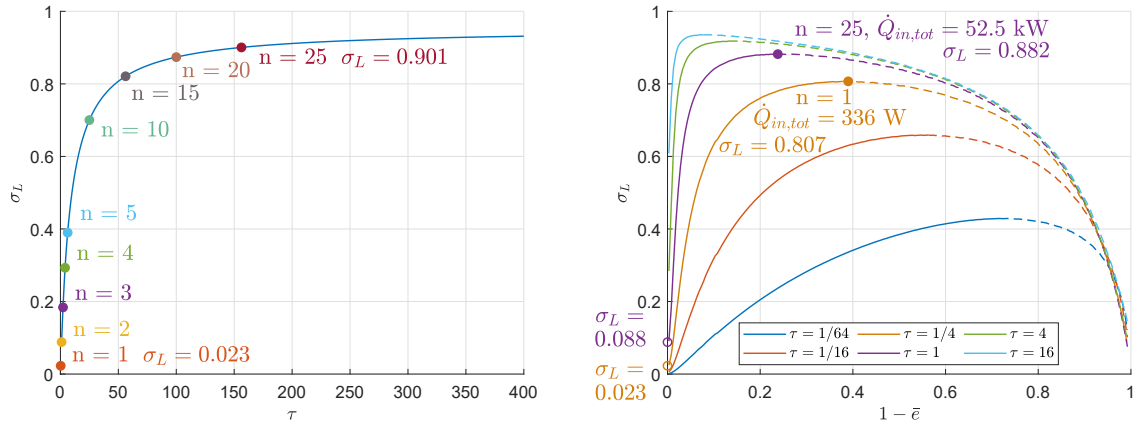

(a) (b)

Figure 7: Performance charts applied to the example case: a) latent charging ratio of the example for different amount of compartments n for an input power of $\dot{Q}_{in}$ = 336 W in absence of fins, and b) charging ratio σ_L for different values of the dimensionless time scale τ for a fin aspect ratio AR_{fin} = 0.01. The markers in b) indicate 1) the low charging ratio for an unfinned design (hollow circles), and 2) the highest possible charging ratio for a finned design with fin aspect ratio AR_{fin} = 0.01 (plain circles).

$$Pe = \frac{\langle v \rangle H}{\alpha_w} = \frac{\dot{Q}_{in} / \rho_w c_w L_z (T_\infty - T_m)}{\alpha_w} = 2.32, \tag{41}$$

and

$$\tau = \frac{\mathrm{AR}_{xy}}{Pe} \cdot \frac{1 + Ste}{\bar{k}_w Ste} = 156.25, \tag{42}$$

which corresponds to a charging ratio of $\sigma_L \approx 0.901$ (see Fig. 7(a)). In other words, a very high fraction of the available heat will effectively get to be stored, even without using highly conductive fins, as long as the compartments are being charged at a low rate[7].

Finally, consider the same storage charged with a much higher total input power[8] of $\dot{Q}_{in,tot}$ = 52 500 W. With n = 25, the compartment input power becomes $\dot{Q}_{in}$ = 1050 W. This changes the compartment Péclet number, the value of τ (using Eq. (17), and (22)), and therefore the charging ratio as follows: Pe = 362.07, τ = 1 and σ_L = 0.088 in absence of fins (see Fig. 7(b) for $\bar{e}$ = 1).

As was already stated in the previous section, faster charging the compartments goes at the cost of less effectively storing the available input power. However, the charging ratio can be significantly elevated by inserting low aspect ratio metal fins. Inserting fins with width equal to the minimum width, i.e. $b_f = b_{f,min}$, results in a minimum fin aspect ratio of AR_{fin} = 0.01. The highest charging performance is reached for $\bar{e}$ = 0.762 and reaches σ_L = 0.882, which is about a factor ten higher than the storage without fins (see Fig. 7(b)). The example case therefore confirms that 1) reducing the compartment height and increasing the number of compartments combined with parallel charging increases the charging performance significantly, and 2) slowly

[7]It was found by numerical simulation that the combined latent and sensible charging ratio is higher and reaches $\sigma \approx 0.953$.

[8]Note that again the input power is chosen such that the combined charging and storage performance is easily derived from the limited set of performance maps, i.e. Fig. 3 and Fig. 4, without the need for interpolation.

charging individual compartments increases the fraction of effectively stored heat. In addition, the example shows that the fin fraction can be optimized to maximize the charging effectiveness.

5 Conclusions

A general dimensionless framework for the LHS performance analysis was created for latent heat storages with cuboid compartments enhanced by straight highly conductive metal fins. The LHS consists of stacked identical storage compartments and is charged by a constant heat input by means of a hot water flow. The individual storage compartments were modelled by numerical simulations to calculate their combined storage and charging performance, and their trends where captured by dimensionless performance maps. It was shown that reducing the compartment heights is the best way to increase the charging performance. Also, including highly conductive metal fins allows the charging performance to be increased, however, at the cost of a lower storage capacity. The performance trends all showed a Pareto front, indicating the trade-off between storage capacity and charging performance for fin volume fractions under a given upper limit. Decreasing the fin aspect ratio by reducing the fin width is beneficial for the charging power for equal metal volume fractions. Further, it was demonstrated that slowly and simultaneously charging the LHS compartments increases the effectiveness of storing the available heat.

6 Acknowledgments

This research is funded by the internal KU Leuven C1-funding. The computational resources and services used in this work were provided by the VSC (Flemish Supercomputer Center), funded by the Research Foundation Flanders (FWO) and the Flemish Government department EWI. Maarten Blommaert is a postdoctoral research fellow of the Research Foundation - Flanders (FWO) and VITO, the Flemish Institute for Technological Research.

References

[1] B. Zalba, J. M. Marn, L. F. Cabeza, and H. Mehling, "Review on thermal energy storage with phase change: materials, heat transfer analysis and applications," Applied Thermal Engineering, vol. 23, pp. 251–283, 2003.

[2] L. Fan and J. Khodadadi, "Thermal conductivity enhancement of phase change materials for thermal energy storage: A review," Renewable and Sustainable Energy Reviews, vol. 15, pp. 24–46, 2011.

[3] P. Lamberg and K. Siren, "Approximate analytical model for solidification in a finite PCM storage with internal fins," Applied Mathematical Modelling, vol. 27, pp. 491–513, 2003.

[4] R. Akhilesh, A. Narasimhan, and C. Balaji, "Method to improve geometry for heat transfer enhancement in PCM composite heat sinks," International Journal of Heat ans Mass Transfer, vol. 48, pp. 2759–2770, 2005.

[5] K. Nayak, S. Saha, K. Srinivasan, and P. Dutta, "A numerical model for heat sinks with phase change materials and thermal conductivity enhancers," International Journal of Heat ans Mass Transfer, vol. 49, pp. 1833–1844, 2006.

[6] F. Agyenim, P. Eames, and M. Smyth, "A comparison of heat transfer enhancement in a medium temperature thermal energy storage heat exchanger using fins," Solar Energy, vol. 83, pp. 1509–1520, 2009.

[7] S. Saha and P. Dutta, "Heat transfer correlations for PCM-based heat sinks with plate fins," Applied Thermal Engineering, vol. 30, pp. 2485–2491, 2010.

[8] B. Kamkari and H. Shokouhmand, "Experimental investigation of phase change material melting in rectangular enclosures with horizontal partial fins," International Journal of Heat and Mass Transfer, vol. 78, pp. 839–851, 2014.

[9] S. Mat, A. A. Al-Abidi, K. Sopian, M. Sulaiman, and A. T. Mohammad, "Enhance heat transfer for PCM melting in triplex tube with internalexternal fins," Energy Conversion and Management, vol. 74, pp. 223–236, 2013.

[10] M. J. Hosseini, M. Rahimi, and R. Bahrampoury, "Thermal analysis of PCM containing heat exchanger enhanced with normal annular fines," Mechanical Sciences, vol. 6, pp. 221–234, 2015.

[11] R. Pakrouh, M. J. Hosseini, and A. A. Ranjbar, "A parametric investigation of a PCM-based pin fin heat sink," Mechanical Sciences, vol. 6, pp. 65–73, 2015.

[12] R. Pakrouh, M. Hosseini, A. Ranjbar, and R. Bahrampoury, "A numerical method for PCM-based pin fin heat sinks optimization," Energy Conversion and Management, vol. 103, pp. 542–552, 2015.

[13] S. Ziaei, S. Lorente, and A. Bejan, "Morphing tree structures for latent thermal energy storage," Journal of Applied Physics, vol. 117, 2015.

[14] F. Jorissen, "Verbetering van PCM thermische opslagconcepten en optimaal gebruik in combinatie met warmtepomp," Master's thesis, KU Leuven, 2012-2013.

[15] A. Pizzolato, A. Sharma, K. Maute, A. Sciacovelli, and V. Verda, "Topology optimization for heat transfer enhancement in Latent Heat Thermal Energy Storage," International Journal of Heat and Mass Transfer, vol. 113, pp. 875–888, 2017.

[16] A. Pizzolato, A. Sharmab, K. Mauteb, A. Sciacovellic, and V. Verda, "Design of effective fins for fast PCM melting and solidification in shell-and-tube latent heat thermal energy storage through topology optimization," Applied Energy, vol. 208, pp. 210–227, 2017.

[17] C. A. Bauer and R. Wirtz, "Thermal Characteristics of a Compact, Passive Thermal Energy Storage Device," in 2000 ASME IMECE: Undergraduate Research and Design in Heat Transfer, 2000.

[18] Y. Tian and C. Zhao, "A numerical investigation of heat transfer in phase change materials (PCMs) embedded in porous metals," Energy, vol. 36, pp. 5539–5546, 2011.

[19] M. Almajali, K. Lafdi, and P. Prodhomme, "Effect of copper coating on infiltrated PCM/foam," Energy Conversion and Management, vol. 66, pp. 336–342, 2013.

[20] W. Li, H. Wan, H. Lou, Y. Fu, F. Qin, and G. He, "Enhanced thermal management with microencapsulated phase change material particles infiltrated in cellular metal foam," Energy, vol. 127, pp. 671–679, 2017.

[21] A. Pizzolato, Topology optimization for energy problems. PhD thesis, Politecnico Di Torino, 2018.

[22] J. Kośny, PCM-Enhanced Building Components: An Application of Phase Change Materials in Building Envelopes and Internal Structures. Springer, 2015.

[23] P. B. Salunkhe and P. S. Shembekar, "A review on effect of phase change material encapsulation on the thermal performance of a system," Renewable and Sustainable Energy Reviews, vol. 16, pp. 5603–5616, 2012.

[24] R. A. Shannaq and M. Farid, "10 - Microencapsulation of phase change materials (PCMs) for thermal energy storage systems," in Advances in Thermal Energy Storage Systems (L. F. Cabeza, ed.), Woodhead Publishing Series in Energy, pp. 247 – 284, Woodhead Publishing, 2015.

[25] D. Groulx, "The rate problem in solid-liquid phase change heat transfer: Efforts and questions towards heat exchanger design rules," in Proceedings of the 16th International Heat Transfer Conference, IHTC-16, 2018.

[26] B. Peremans, M. Blommaert, J. Diriken, and M. Baelmans, "Limits of latent heat storage charging," in Proceedings of the 2nd Thermal and Fluid Engineering Conference, TFEC2017, American Society of Thermal and Fluids Engineers, 2017.

[27] B. Peremans, M. Blommaert, J. Diriken, and M. Baelmans, "Towards energy efficient latent heat storage tanks with heat transfer fluid channels and finite inlet power," in Proceedings of the 16th International Heat Transfer Conference, IHTC-16, 2018.

[28] E. Vasquez, F. Degasperi, L. Morita, M. Gongora Rubio, and R. Giudici, "Development of a micro-heat exchanger with stacked plates using ltcc technology," Brazilian Journal of Chemical Engineering, vol. 27, pp. 483–497, 06 2010.

[29] C. Pistoresi, Y. Fan, and L. Luo, "Numerical study on the improvement of flow distribution uniformity among parallel mini-channels," Chemical Engineering and Processing: Process Intensification, vol. 95, pp. 63–71, 2015.

[30] T. Van Oevelen, Optimal Heat Sink Design for Liquid Cooling of Electronics. PhD thesis, KU Leuven, 2014.

[31] F. P. Incropera, D. P. Dewitt, T. L. Bergman, and A. S. Lavine, Fundamentals of Heat and Mass Transfer. Wiley, 2006.

[32] M. Jourabian and M. Farhadi, "Melting of nanoparticles-enhanced phase change material (NEPCM) in vertical semicircle enclosure: numerical study," Journal of Mechanical Science and Technology, vol. 29, 06 2015.

[33] J. Vogel, Influence of natural convection on melting of phase change materials. PhD thesis, Universität Stuttgart, 2018.